Pharmacogn. Res., 2026; 18(3):829-842.
https://www.phcogres.com

Original Article

Combining Experimental and Computational Approaches to Elucidate the Anti-T2DM Potential of *Eriobotrya japonica* Flower: *In vitro* Enzyme Inhibition, Network Pharmacology, Molecular Docking, and Molecular Dynamics Simulation

Hanhua Wang[1,*], Sisi Zeng[1], Yanyue Wang[2]

[1]College of Traditional Chinese Medicine, Zhejiang Pharmaceutical University, Ningbo, CHINA.
[2]Department of Mathematics and Information Technology, The Education University of Hong Kong, Hong Kong, SAR CHINA.

ABSTRACT

Objectives: To investigate the anti-T2DM potential and mechanism of *Eriobotrya japonica* (loquat) flower using an integrated approach combining in vitro assays, network pharmacology, molecular docking, and Molecular Dynamics (MD) simulation. **Materials and Methods:** The α-glucosidase inhibitory activity of 70% ethanol extracts from 18 batches of loquat flowers was evaluated. Active components and targets were identified via network pharmacology, with core targets discerned through Protein-Protein Interaction (PPI) network analysis. Gene Ontology (GO) and Kyoto Encyclopedia of Genes and Genomes (KEGG) enrichment analyses were performed. Molecular docking validated interactions between key components and targets, and their ADMET properties were predicted. MD simulation assessed the binding stability and affinity of the quercetin-AKT1 complex. **Results:** All extracts inhibited α-glucosidase concentration-dependently. Network pharmacology identified 8 active components (*e.g.*, Quercetin, Ursolic acid) and 196 common targets, including core targets TP53, AKT1, STAT3, and TNF. Enrichment analyses implicated pathways in lipid metabolism, atherosclerosis, and hormone response. Molecular docking confirmed stable binding (energy < -7 kcal/mol). ADMET predictions indicated favorable pharmacokinetics. MD simulations demonstrated exceptional stability and strong binding affinity (-43.06 kcal/mol) for the quercetin-AKT1 complex, primarily driven by van der Waals interactions. **Conclusion:** Loquat flower exerts anti-diabetic effects via multi-component, multi-target, and multi-pathway mechanisms, involving enzyme inhibition and modulation of insulin resistance and inflammation pathways. MD simulations provided atomic-level validation of the key interaction, robustly supporting the proposed multifaceted mechanism.

Keywords: α-glucosidase Inhibition, Bioinformatics, *Eriobotrya japonica* Flower, Molecular Docking, Molecular Dynamics Simulation, Network Pharmacology, Type 2 Diabetes Mellitus.

Correspondence:
Mr. Hanhua Wang
College of Traditional Chinese Medicine, Zhejiang Pharmaceutical University, Ningbo-315503, CHINA.
Email: 178191012@QQ.com

Received: 12-01-2026;
Revised: 02-02-2026;
Accepted: 27-04-2026.

INTRODUCTION

With the improvement of living standards and changes in lifestyle, the global prevalence of Diabetes Mellitus (DM) continues to increase at an alarming rate. According to authoritative projections, the number of diabetic patients is expected to reach 783.2 million by 2045 (Sun *et al.*, 2022). DM is an endocrine and metabolic disorder characterized by chronic hyperglycemia, with Type 2 Diabetes Mellitus (T2DM) accounting for more than 90% of all cases (Luo *et al.*, 2023). Current treatments for T2DM, besides insulin injections, include oral hypoglycemic agents such as biguanides and α-glucosidase inhibitors (Araki *et al.*, 2021). However, these medications are associated with adverse effects, underscoring the need to identify efficient and low-toxicity natural compounds for adjuvant therapy. Inhibiting α-glucosidase can delay carbohydrate digestion and absorption, thereby reducing postprandial blood glucose elevation. Consequently, *in vitro* α-glucosidase inhibition assays have become a rapid and convenient method for evaluating hypoglycemic activity (Xiong *et al.*, 2025; Chen *et al.*, 2023).

Eriobotrya japonica Lindl. (loquat) flower, the dried flower buds and inflorescences of the Rosaceae plant, is a Traditional Chinese Medicine (TCM) with a mild flavor and neutral nature. It is known to act on the lung meridian, functioning to clear the nasal passages, dispel wind, and relieve cough. It is commonly used in folk medicine to treat conditions such as lung-heat-induced

DOI: 10.5530/pres.20260221

cough in children, as well as persistent cough in the elderly and chronic patients (Wang *et al.*, 2019). In fruit cultivation, the routine practice of flower thinning generates substantial by-products of loquat flowers. Notably, these by-products hold value as a food source, with a tradition of consumption in regions like Fujian, Zhejiang, and Guangdong, where they are prepared as beverages, soups, porridges, or stewed dishes. This potential was formally recognized in 2019 when loquat flower was approved as a novel food ingredient by the National Health Commission of China (National Health Commission of the People's Republic of China, 2019). Previous research by our group has demonstrated that loquat flower possesses antitussive, expectorant (Wang *et al.*, 2019), antibacterial, and anti-inflammatory activities (Wang *et al.*, 2018). Other studies suggest that its flavonoids may help prevent cardiovascular diseases and diabetes (Zeka *et al.*, 2017). While the significant hypoglycemic effects of loquat leaf, a plant from the same genus, have been reported (Wahjudi *et al.*, 2017; Chen *et al.*, 2017), the specific active constituents and mechanisms underlying the anti-diabetic properties of loquat flower remain unclear.

With the rapid advancement of multi-omics technologies and the widespread application of public databases, bioinformatics and network pharmacology approaches—which rely on computational and mathematical methods to analyze biological data—have demonstrated significant potential in drug discovery, including target identification and mechanism elucidation (Zhang *et al.*, 2023; zhai *et al.*, 2023; Ma *et al.*, 2025). Reflecting the multi-component, multi-target, and multi-pathway characteristics of herbal medicine, this study integrates experimental and computational strategies, including *in vitro* enzyme inhibition, network pharmacology, molecular docking, and Molecular Dynamics (MD) simulation, to investigate the pharmacodynamic material basis and underlying mechanisms of loquat flower against T2DM. Furthermore, to overcome the static limitations of molecular docking and rigorously validate the binding interactions, MD simulation and MM/GBSA free energy calculations were conducted, providing atomic-level insights into binding stability and affinity. The findings aim to provide a scientific basis for the development of loquat flower as a functional food for T2DM management.

MATERIALS AND METHODS

Materials and Reagents

A total of eighteen batches of loquat flowers were collected from multiple distinct origins, as detailed in Table 1. The samples were collected from sixteen locations within China and two international sites. α-glucosidase (Batch No. 20231220, Shanghai Shifeng Biotechnology Co., Ltd.); p-Nitrophenyl-α-D-glucopyranoside (PNPG, Shanghai Shifeng Biotechnology Co., Ltd.); Acarbose (AR, Shanghai Shifeng Biotechnology Co., Ltd.); Anhydrous ethanol (AR, Xilong Science & Technology Co., Ltd.); Anhydrous Na_2CO_3 (AR, Sinopharm Chemical Reagent Co., Ltd.); Ultrapure water (self-prepared).

Instruments

DHG-9023A electric thermostatic forced-air drying oven (Shanghai Jinghong Laboratory Equipment Co., Ltd.); Multiskan SkyHigh full-wavelength microplate reader (Thermo Fisher Scientific (China) Co., Ltd.); SB-5200D ultrasonic cleaner (Ningbo Scientz Biotechnology Co., Ltd.); N-1300S-W rotary evaporator (Tokyo Rikakikai Co., Ltd.); LX-2000 cooling water circulation machine (Beijing Coolium Instruments Co., Ltd.); FUJ-V150 diaphragm vacuum pump (Taizhou Tengyuan Tools Co., Ltd.); SQP electronic analytical balance (Thermo Scientific); HH-2S constant temperature water bath (Guohua (Changzhou) Instrument Manufacturing Co., Ltd.).

Sample Preparation

Loquat flowers were dried at 40°C for 90 min and pulverized. A portion of the powder (5.0 g) was extracted with 50 mL of 70% ethanol using ultrasound (200 W) for 30 min and then filtered. The extraction was repeated twice, and the combined filtrates were concentrated under reduced pressure. The resulting extract (60 mg) was dissolved in Phosphate-Buffered Saline (PBS) and serially diluted to create the required concentration gradients for subsequent assays.

Determination of α-glucosidaseInhibition Rate

The assay was performed with modifications based on the method described by Xiong *et al.* (2025). Briefly, 50 µL of loquat flower extract at different concentrations (1.0, 2.0, 3.0, 4.0, and 5.0 mg/mL) was mixed with 50 µL of PBS and 50 µL of α-glucosidase solution (2.5 U/mL). The mixture was incubated at 37°C for 15 min, followed by the addition of 50 µL of 1.0 mmol/L PNPG solution and further incubation for 30 min. The reaction was terminated by adding 50 µL of 1.0 mol/L Na_2CO_3 solution. Absorbance was measured at 405 nm. A blank control (replacing the extract with distilled water) and a negative control (replacing the α-glucosidase solution with distilled water) were prepared simultaneously. The inhibition rate (%) was calculated as: Inhibition rate (%) = $[1 - (A_1 - A_2)/A_0] \times 100\%$, where A_0 is the absorbance of the blank control, A_1 is the absorbance of the experimental group, and A_2 is the absorbance of the negative control.

Statistical Analysis

All *in vitro* α-glucosidase inhibition assays were performed in three independent replicates (n=3). The data are presented as Mean ± Standard Deviation (SD). The half-maximal Inhibitory Concentration (IC_{50}) for each batch was determined by fitting the concentration-response data to a non-linear regression model using GraphPad Prism 9.0 software.

Screening of Active Ingredients and Protein Targets

Active ingredients of loquat flower were retrieved from the Traditional Chinese Medicine Systems Pharmacology Database and Analysis Platform (TCMSP, https://www.tcmsp-e.com/tcmsp.php) and supplemented by literature review (Ru *et al.*, 2024). Compounds with higher activity were screened under the conditions of Oral Bioavailability (OB) ≥ 30% and Drug-Likeness (DL) ≥ 0.18. The TCMSP database was utilized to identify targets corresponding to the small molecules, and the UniProt database (http://www.uniprot.org/uploadlists/) was employed to standardize the target names into official gene symbols (Consortium, 2023).

Collection of Disease-related Targets

Disease-associated targets were acquired from four databases: CTD (http://ctdbase.org/), OMIM (https://omim.org/), Genecards (https://www.genecards.org/), and Drugbank (https://www.drugbank.ca/) (Davis *et al.*, 2023; Li *et al.*, 2023). Duplicate and false-positive targets were removed. The Venny 2.1 online tool (https://bioinfogp.cnb.csic.es/tools/venny/) was used to obtain the intersection between loquat flower targets and disease-related targets. Cytoscape software (v3.10.1) was applied for network visualization, and topological analysis was performed to calculate the degree value of each node.

Protein-Protein Interaction (PPI) Network Construction and Core Target Analysis

To investigate the potential key targets of loquat flower and their interactions, a PPI network was constructed using the STRING online platform (https://cn.stringdb.org/) (Szklarczyk *et al.*, 2025). The protein species was set to Homo sapiens with a medium confidence score threshold (0.400). Finally, the Cytohubba plugin was used to rank the targets by the Maximal Clique Centrality (MCC) algorithm (Yan *et al.*, 2025). The top 10 targets from the PPI network were identified as core targets.

Gene Ontology (GO) Functional Annotation and Kyoto Encyclopedia of Genes and Genomes (KEGG) Pathway Enrichment Analysis

The GO database (http://www.geneontology.org) was used to analyze the enriched biological functions in terms of Cellular Components (CC), Molecular Functions (MF), and Biological Processes (BP), providing an overview of the biological functions, pathways, and locations of the genetic information. KEGG (https://www.genome.jp/kegg/), a core database for functional genomics, integrates genomic, chemical, and systems biological data to support gene function annotation and pathway enrichment analysis. Based on the preprocessed core targets, Metascape (https://metascape.org/) was employed for GO and KEGG analyses to systematically decipher the functional characteristics of CC, MF, BP, and signaling pathways (Zhou *et al.*, 2019). The resulting data were imported into a bioinformatics data analysis and visualization platform (http://www.bioinformatics.com.cn/) to generate bubble diagrams.

Molecular Docking and Analysis of Absorption, Distribution, Metabolism, Excretion, and Toxicity (ADMET)

The top four active ingredients of loquat flower, ranked by their degree values, were selected for molecular docking. Their three-dimensional molecular structures (in *Mol2 format) were obtained from the PubChem database (https://pubchem.ncbi.nlm.nih.gov/) (Kim *et al.*, 2025). The 3D structures of the top four target proteins (in *PDB format) were downloaded from the RCSB PDB database (https://www.rcsb.org/) (Flachsenberg *et al.*, 2024). The original ligand was removed from the protein crystal structure using PyMOL. Subsequent protein preparation was performed with AutoDock tools, which involved the removal of water molecules, the addition of explicit hydrogen atoms, and the conversion of the file to the *pdbqt format. For the small molecule ligands, rotatable bonds were defined, and the molecules were also saved in the *pdbqt format. The binding site was defined based on the spatial coordinates of the original ligand. Molecular docking was then carried out using AutoDock Vina to identify the binding pose with the highest predicted affinity. The resulting complexes were visualized with PyMOL, and the specific ligand-protein interactions were analyzed and visualized in two dimensions using Discovery Studio.

The drug-like properties of the active ingredients from loquat flower were predicted using the SwissADME online platform (http://www.swissadme.ch/). The chemical structures of these active ingredients were input into the platform for ADMET property analysis. The toxicity of the active ingredients was further evaluated using Pro-Tox 3.0 (https://tox.charite.de/).

MD Simulation

A 100 ns all-atom MD simulation was performed on the complex using Gromacs 2020.6 software. The CHARMM27 force field was employed for the protein, while force field parameters for quercetin were generated using the GAFF force field. The system was set up at a temperature of 293.15 K, utilizing the TIP3P water model, with Na^+/Cl^- ions added to neutralize the system charge. Energy minimization was first conducted to eliminate unfavorable steric clashes, sequentially using the conjugate gradient algorithm followed by the steepest descent method for optimization. Following energy minimization, a full MD production simulation was carried out. Based on the stable trajectory from the MD simulation (90-100 ns), the binding free energy (ΔG_{bind}) between the protein and ligand was calculated using the MM/GBSA method, as described by Equation 1:

$$\Delta G_{bind} = \Delta G_{complex} - (\Delta G_{receptor} + \Delta G_{ligand})$$
$$= \Delta E_{internal} + \Delta E_{VDW} + \Delta E_{elec} + \Delta G_{GB} + \Delta G_{SA} \quad (1)$$

Here, $E_{intenal}$, E_{VDW} and ΔE_{elec} represent the internal energy (comprising bond, angle, and dihedral energies), van der Waals interactions, and electrostatic interactions in the gas phase, respectively. ΔG_{GB} and ΔG_{SA} denote the solvation free energy, corresponding to the polar (calculated using the GB model with igb=5) and non-polar contributions, respectively. The non-polar solvation energy was calculated using the equation $\Delta G_{SA} = 0.0072 \times \Delta SASA$. Entropic contributions were not considered in this study due to high computational costs and associated low accuracy.

RESULTS

In vitro Experimental Results

α-Glucosidase hydrolyzes glycosidic bonds to release glucose. Inhibition of its activity can interfere with glucose conversion, thereby significantly reducing postprandial blood glucose levels (Zhang *et al.*, 2025). As shown in Table 2, the IC_{50} values for each sample were calculated from dose-response curves at five concentrations, and the inhibition rates at an intermediate concentration (3.0 mg/mL) are also provided. All samples exhibited concentration-dependent inhibitory activity. Sample L12 showed the strongest inhibition, with an IC_{50} of 1.009 mg/mL and an inhibition rate of 68.82% at 3.0 mg/mL. Samples L11, L14, and L16 also demonstrated relatively strong activity, with IC_{50} values below 2 mg/mL. The IC_{50} values across the 18 batches varied considerably, ranging from 1.009 mg/mL to over 5.000 mg/mL, which represents a greater than five-fold difference between the most and least active samples. This considerable variation in IC_{50} values suggests that the α-glucosidase inhibitory activity of loquat flowers is influenced by geographical origin.

Identification of Putative Active Compounds and Their Potential Targets in Loquat Flower for Anti-T2DM

As the TCMSP database does not include loquat flower, six active components of loquat flower and 376 related targets were initially screened based on previous research (Wang *et al.*, 2019) and references (Duan *et al.*, 2025; Huang *et al.*, 2025), considering OB and DL. However, due to the recognized limitations of *in silico* ADME models in accurately predicting the properties of natural products (*e.g.*, triterpenoids, saponins) and to adhere to the holistic principle of TCM (Xie *et al.*, 2023; Odhiambo *et al.*, 2025), we supplemented our compound pool with key bioactive components of loquat flower (such as ursolic acid (Zhu *et al.*, 2022), oleanolic acid (Zhu *et al.*, 2022), corosolic acid (Yamada *et al.*, 2008), and maslinic acid (Sabarathinam and Satheesh, 2025)) that have documented hypoglycemic activity, irrespective of their OB and DL values. Ultimately, eight active components of loquat flower and 411 related targets were obtained. Subsequently, T2DM-related targets were collected from four databases: CTD, OMIM, Genecards, and DrugBank. After removing duplicates, a total of 21,555 disease targets were identified, as shown in Figure 1A. There were 196 overlapping targets between the active components of loquat flower and T2DM, as illustrated in Figure 1B. The relationships between the eight active components of loquat flower for anti-T2DM and the 196 overlapping targets were visualized using Cytoscape software, presented in Figure 1C.

Construction of The PPI Network and Identification of Core Targets

To explore the molecular mechanism of loquat flower against T2DM, the 196 overlapping targets were imported into the STRING database to construct a PPI network. The resulting network contained 187 nodes and 4021 edges, with an average node degree of 43. The PPI network data from the STRING platform were then imported into Cytoscape for visualization, as shown in Figure 1D. Finally, the top 10 core targets were selected using the Degree method in the CytoHubba plugin, including TP53, AKT1, STAT3, TNF, IL6, ESR1, MAPK1, IL1B, CASP3, and BCL2, as depicted in Figure 1E.

GO and KEGG Pathway Enrichment Analysis

GO and KEGG enrichment analyses were performed on the 196 overlapping targets using the Metascape database, and the results were visualized via the bioinformatics platform. As shown in Figures 2A-C, only the top 10 enriched terms are displayed for BP, CC, and MF in the GO analysis. In BP, targets were

Table 1: Geographical origins of loquat flower samples (L1-L16: China; L17: Japan; L18: Laos).

Sample ID	Origin (City/Region)	Sample ID	Origin (City/Region)
L1	Bozhou, Anhui	L10	Chengdu, Sichuan
L2	Zhangzhou, Fujian	L11	Ya'an, Sichuan
L3	Nanning, Guangxi	L12	Ninghai, Zhejiang
L4	Yulin, Guangxi	L13	Ningbo, Zhejiang
L5	Guangzhou, Guangdong	L14	Xiangshan, Zhejiang
L6	Meizhou, Guangdong	L15	Hangzhou, Zhejiang
L7	Foshan, Guangdong	L16	Quzhou, Zhejiang
L8	Nanjing, Jiangsu	L17	Chiba Prefecture, Japan
L9	Suzhou, Jiangsu	L18	Luang Prabang, Laos

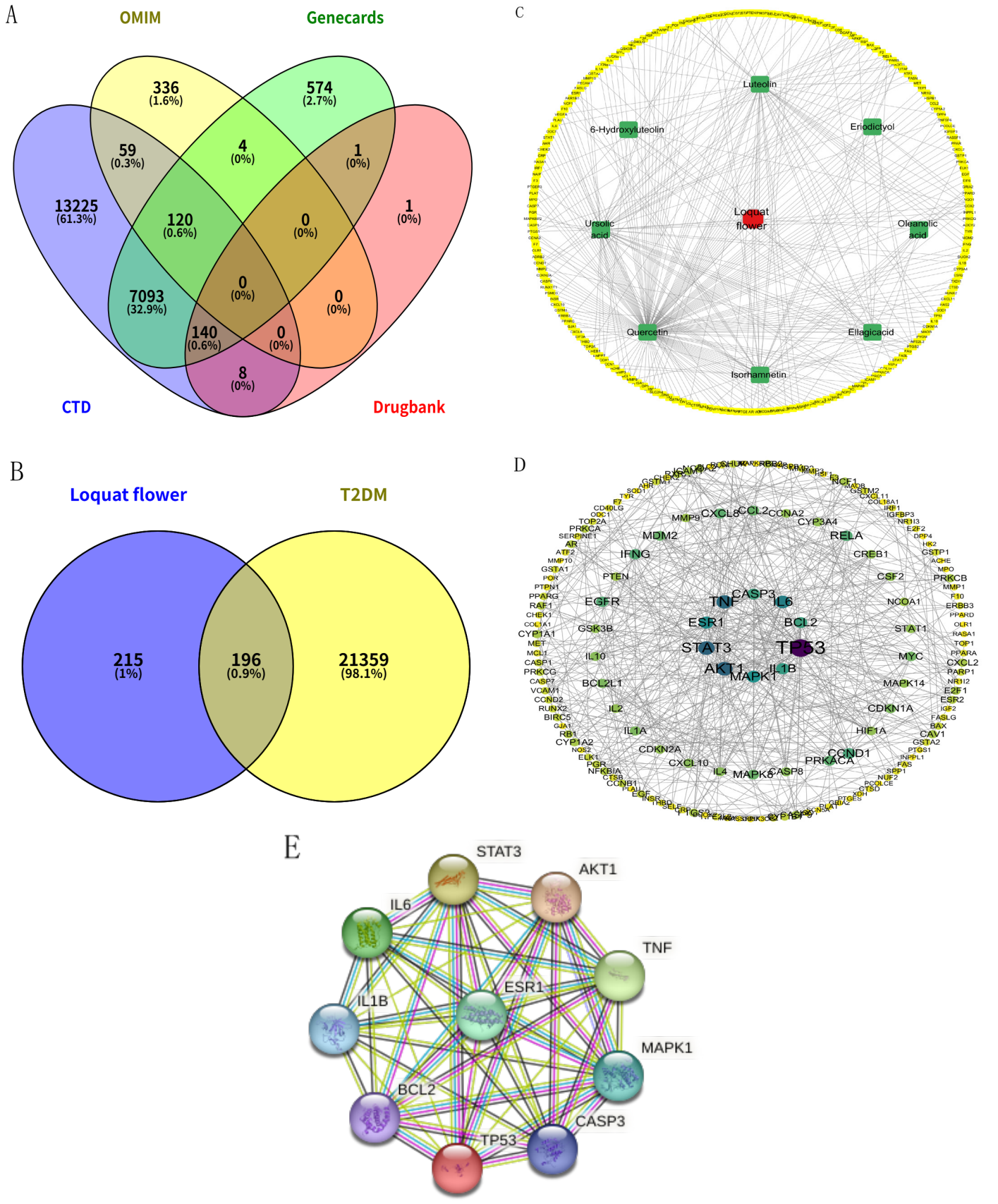

Figure 1: Screening of core targets of loquat flower against T2DM. A. Venn diagram of T2DM targets collected from different databases. B. Venn diagram of the overlapping targets between loquat flower and T2DM. C. The compound-target interaction network (Green and yellow nodes represent the active compounds and disease targets, respectively). D. PPI network of the common target genes (The inner-to-outer arrangement of the circle indicates the strength of protein binding interactions, and the connecting lines represent PPIs). E. The core targets identified by CytoHubba.

Table 2: Summary of α-glucosidase inhibitory activity.

Sample ID	α-glucosidase inhibitory activity		Sample ID	α-glucosidase inhibitory activity	
	IC_{50} (mg/mL)	Inhibition at 3.0 mg/mL (%)		IC_{50} (mg/mL)	Inhibition at 3.0 mg/mL (%)
L1	2.629	54.28±1.39	L 10	4.271	41.86±1.82
L2	4.301	40.86±1.82	L 11	1.276	64.10±2.31
L 3	>5.000	30.68±0.59	L 12	1.009	68.82±1.07
L 4	>5.000	29.46±1.54	L 13	3.847	42.65±1.89
L 5	3.583	45.97±2.33	L 14	1.98	58.62±2.73
L 6	3.198	48.32±1.28	L 15	2.497	55.88±2.32
L 7	3.907	40.92±1.25	L 16	1.995	57.63±1.67
L 8	3.946	40.83±1.89	L17	>5.000	27.10±1.46
L 9	2.991	50.11±1.28	L18	4.536	38.43±1.38

significantly enriched in processes such as "Stress Response & Cell Fate Decision", "Cell Proliferation, Motility & Cancer", "Hormone & Metabolic Regulation", and "Development & Tissue Homeostasis". For CC, targets were primarily enriched in "Signal Transduction Platforms", "Transcriptional Regulation Hub", "Extracellular Matrix & Adhesion", and "Protein Processing & Trafficking". For MF, enrichment was mainly observed in "Cellular Signal Transduction & Regulation", "Gene Transcriptional Regulation", "Immune and Inflammatory Response", and "Cellular Metabolism". The KEGG pathway analysis displayed the top 10 enriched pathways, including "Pathways in cancer', "Human cytomegalovirus infection", "Lipid and atherosclerosis", and "Chemical carcinogenesis - receptor activation", as shown in Figure 2D.

Molecular Docking Validation and ADMET Analysis

Based on the core targets identified above and the Cytoscape visualization results, the binding energies between loquat flower's active components (quercetin, ursolic acid, luteolin, isorhamnetin) and the T2DM-related core targets (TP53, AKT1, STAT3, TNF) were calculated using the CB-DOCK2 web server (https://cadd.labshare.cn/cb-dock2/index.php, accessed on 30 June 2025) (Zhou *et al.*, 2025). All binding energies were less than -7 kcal/mol (Table 3). A lower binding energy indicates a more stable conformation when the drug molecule (ligand) binds to the target. The docking results were imported into PyMOL software for visualization; the molecular docking diagrams are shown in Figure 3.

The evaluation of ADMET (Absorption, Distribution, Metabolism, Excretion, and Toxicity) properties is an indispensable core assessment module in natural drug research and development (Singh *et al.*, 2025). ADMET analysis was performed using the SwissADME database, and the results indicated that the key active components of loquat flower possess favorable pharmacokinetic properties. As shown in Table 4, the pharmacokinetic analysis of the four active components from loquat flower across multiple prediction models revealed no adverse effects in terms of gastrointestinal absorption, blood-brain barrier penetration, P-glycoprotein substrate characteristics, or human oral absorption. Furthermore, all four active components exhibited favorable biocompatibility in various toxicity prediction models, with no indications of reverse mutation, hepatotoxicity, or other toxic responses. However, in predictions of carcinogenicity and mutagenicity, quercetin and luteolin were indicated as "active." In nephrotoxicity predictions, quercetin, luteolin, and isorhamnetin all showed "active" outcomes, with probability values ranging between 0.62 and 0.64, suggesting potential toxicity risks that warrant further attention.

MD Simulation Analysis

MD simulation was performed on the Quercetin-AKT1 complex, which was selected from molecular docking screening based on its optimal binding energy. The stability of the complex was assessed by analyzing the Root-Mean-Square Deviation (RMSD). The protein backbone converged after approximately 40 ns, fluctuating within a range of about 6 Å, indicating that the protein structure had reached an equilibrium state. Meanwhile, Quercetin exhibited minimal fluctuation (approximately 0.5 Å) throughout the simulation, demonstrating exceptional stability within the binding pocket (Figure 4A). Root-Mean-Square Fluctuation (RMSF) analysis revealed that regions of high flexibility were predominantly located in loop regions or at the terminal ends of the protein. In contrast, the core region where the ligand binds remained rigid, suggesting that the binding did not introduce additional structural instability (Figures 4B and 4C).

The binding free energy calculation indicated a strong binding affinity between Quercetin and AKT1 (ΔG_{bind} = -43.06 ± 0.72 kcal/mol), with van der Waals interactions (ΔE_{vdw} = -47.62 ± 0.62 kcal/mol) identified as the primary driving force. Energy decomposition per residue identified the top 10 amino acid residues contributing most significantly to the binding, including TRP80, TYR272, and LEU210, which collectively form a binding

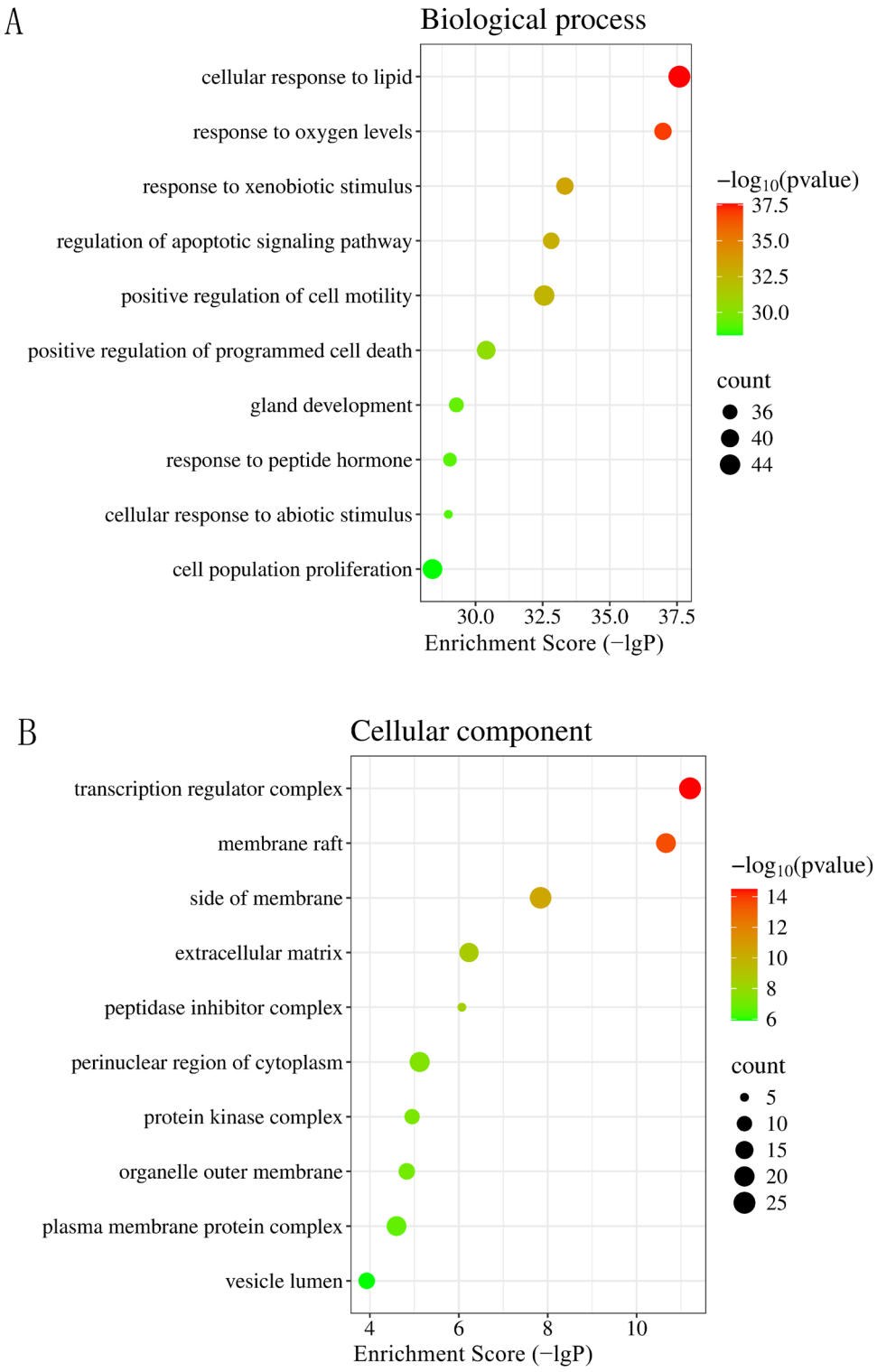
A
Biological process
cellular response to lipid
response to oxygen levels
response to xenobiotic stimulus
regulation of apoptotic signaling pathway
positive regulation of cell motility
positive regulation of programmed cell death
gland development
response to peptide hormone
cellular response to abiotic stimulus
cell population proliferation
30.0
32.5
35.0
37.5
Enrichment Score (−lgP)
−log10(pvalue)
37.5
35.0
32.5
30.0
count
36
40
44
B
Cellular component
transcription regulator complex
membrane raft
side of membrane
extracellular matrix
peptidase inhibitor complex
perinuclear region of cytoplasm
protein kinase complex
organelle outer membrane
plasma membrane protein complex
vesicle lumen
4
6
8
10
Enrichment Score (−lgP)
−log10(pvalue)
14
12
10
8
6
count
5
10
15
20
25

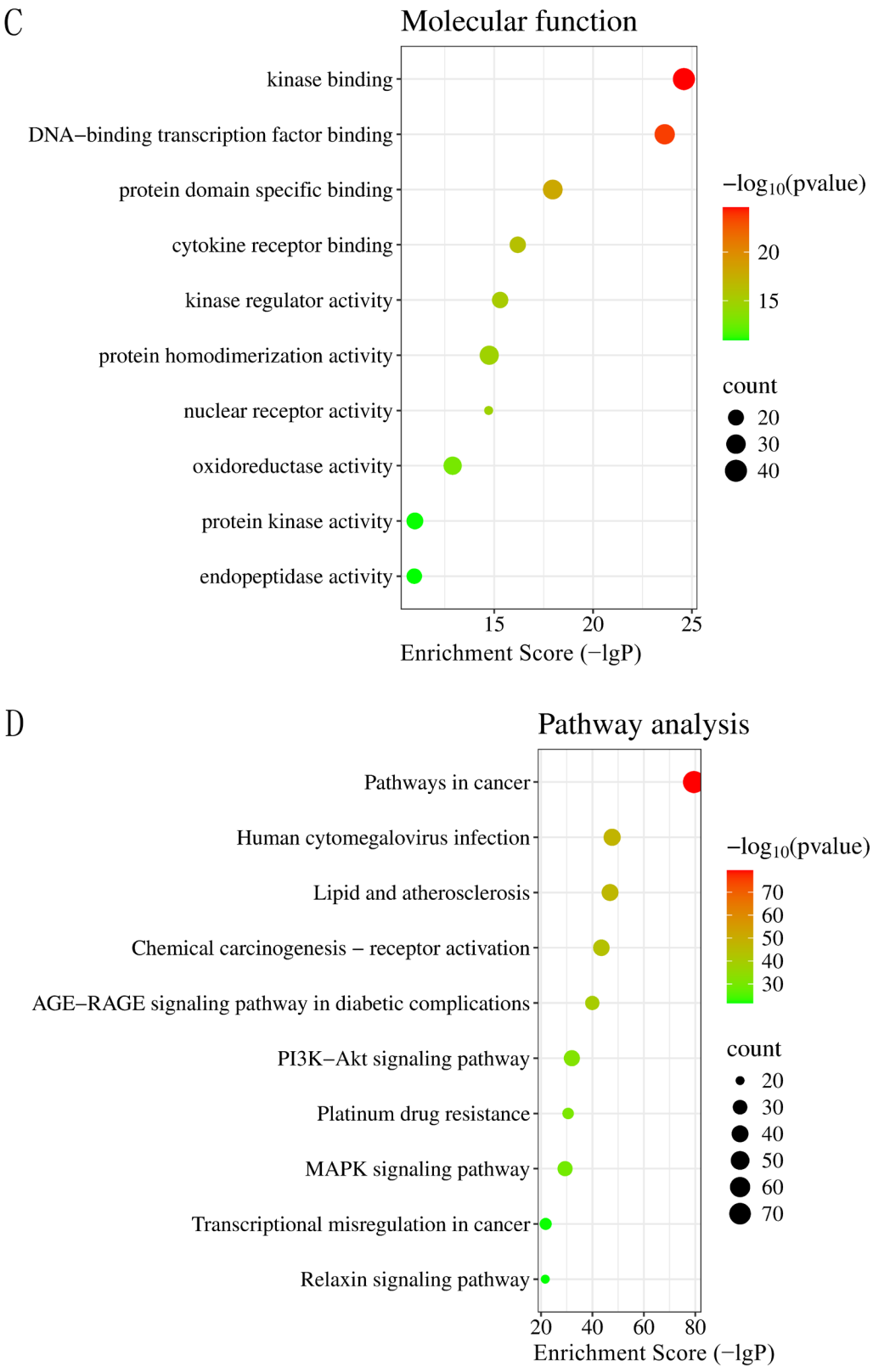

Figure 2: Enrichment analyses of GO and KEGG. A. Top 10 biological processes by enrichment degree in GO analysis. B. Top 10 cellular components by enrichment degree in GO analysis. C. Top 10 molecular functions by enrichment degree in GO analysis. D. Top 10 signaling pathways by enrichment degree in KEGG analysis.

Table 3: Binding energies between active components of loquat flower and core targets.

Target	Binding energy (kcal/mol)			
	Quercetin (MOL000098)	Ursolic acid (MOL000511)	Luteolin (MOL000006)	Isorhamnetin (MOL000354)
TP53	-8.0	-9.9	-7.7	-7.5
AKT1	-9.8	-8.9	-9.8	-9.2
STAT3	-8.0	-7.7	-7.7	-7.6
TNF	-9.1	-7.9	-9.1	-9.0

Notes: The compound identifiers in parentheses (e.g., MOL000098) correspond to the TCMSP database accession numbers. The same identifiers are used consistently throughout all tables for each compound.

Table 4: ADMET analysis of key active components of loquat flower.

Property	Quercetin (MOL000098)	Ursolic acid (MOL000511)	Luteolin (MOL000006)	Isorhamnetin (MOL000354)
GI absorption	High	Low	High	High
BBB permeant	No	No	No	No
P-gp substrate	No	No	No	No
CYP1A2 inhibitor	Yes	No	Yes	Yes
CYP2C19 inhibitor	No	No	No	No
CYP2C9 inhibitor	No	No	No	No
CYP2D6 inhibitor	Yes	No	Yes	Yes
CYP3A4 inhibitor	Yes	No	Yes	Yes
Predicted LD50 ($mg \cdot kg^{-1}$)	159	1190	3919	5000
Hepatotoxicity	Inactive	Active (0.69)	Inactive	Inactive
Nephrotoxicity	Active (0.62)	Inactive	Active (0.62)	Active (0.64)
Carcinogenicity	Active (0.68)	Inactive	Active (0.68)	Inactive
Mutagenicity	Active (0.51)	Inactive	Active (0.51)	Inactive
Cytotoxicity	Inactive	Inactive	Inactive	Inactive

Notes: The numbers in parentheses represent the probability values (ranging from 0 to 1) of predictive confidence. A value greater than 0.5 but less than 0.7 indicates a marginal prediction by the model, suggesting potential risk of the molecule exhibiting this toxicity; a value greater than 0.7 serves as a high-risk alert.

pocket predominantly mediated by hydrophobic interactions (Figure 4D).

Analysis of the final binding mode revealed a stable interaction network, comprising three hydrogen bonds, four hydrophobic interactions, and one critical π-π stacking interaction with TRP80. TRP80 was found to play a central role in both the energy decomposition and the interaction network analyses.

DISCUSSION

This study provides a systematic evaluation of the anti-T2DM potential of loquat flower through a combined experimental and computational approach. The *in vitro* assays demonstrated that extracts from all 18 batches of loquat flower concentration-dependently inhibited α-glucosidase. This selective inhibition is particularly advantageous for a functional food, as it can effectively delay carbohydrate digestion without typically causing significant malabsorption-related discomfort (Li *et al.*, 2025). Notably, significant variation in inhibitory activity was observed among the samples, with IC_{50} values ranging from 1.009 mg/mL to over 5.000 mg/mL. The sample from Ninghai, Zhejiang, China (L12) exhibited the most potent activity. This geographical variation suggests that growing environments may substantially influence the accumulation of active constituents in loquat flowers, providing important experimental evidence for future screening of superior germplasm and standardization of raw materials.

Our integrated approach is consistent with the hypothesis that loquat flower mediates its anti-T2DM effects through a synergistic "multi-component, multi-target, multi-pathway" mode. Eight core components were identified, predominantly flavonoids (*e.g.*, quercetin, luteolin) and triterpenoids (*e.g.*, ursolic acid). The polyhydroxy-substituted structures of the core flavonoids

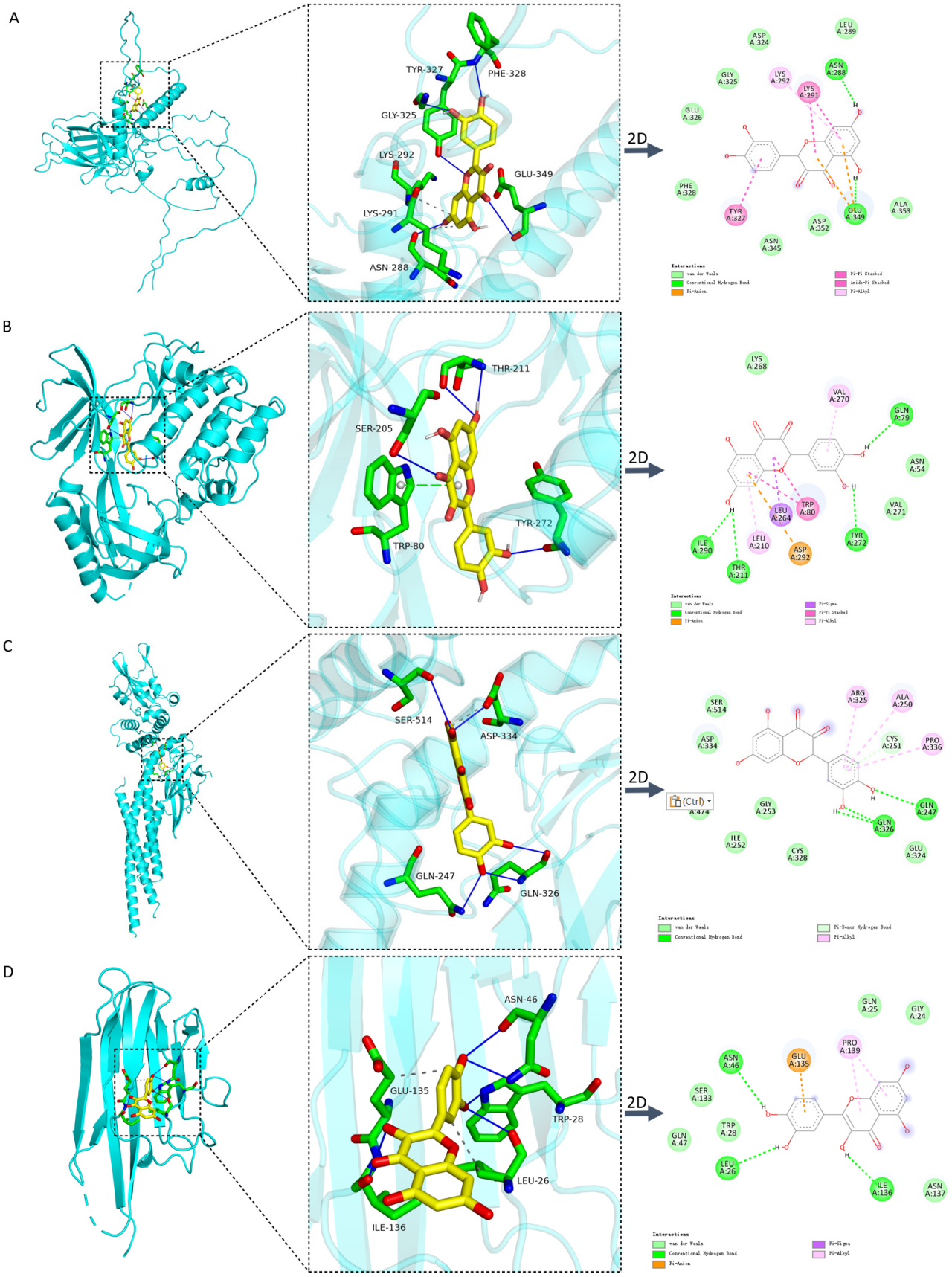

Figure 3: Molecular docking diagrams of quercetin with core targets of T2DM. A Quercetin dock with TP53. B Quercetin dock with AKT1. C Quercetin dock with STAT3. D Quercetin dock with TNF.

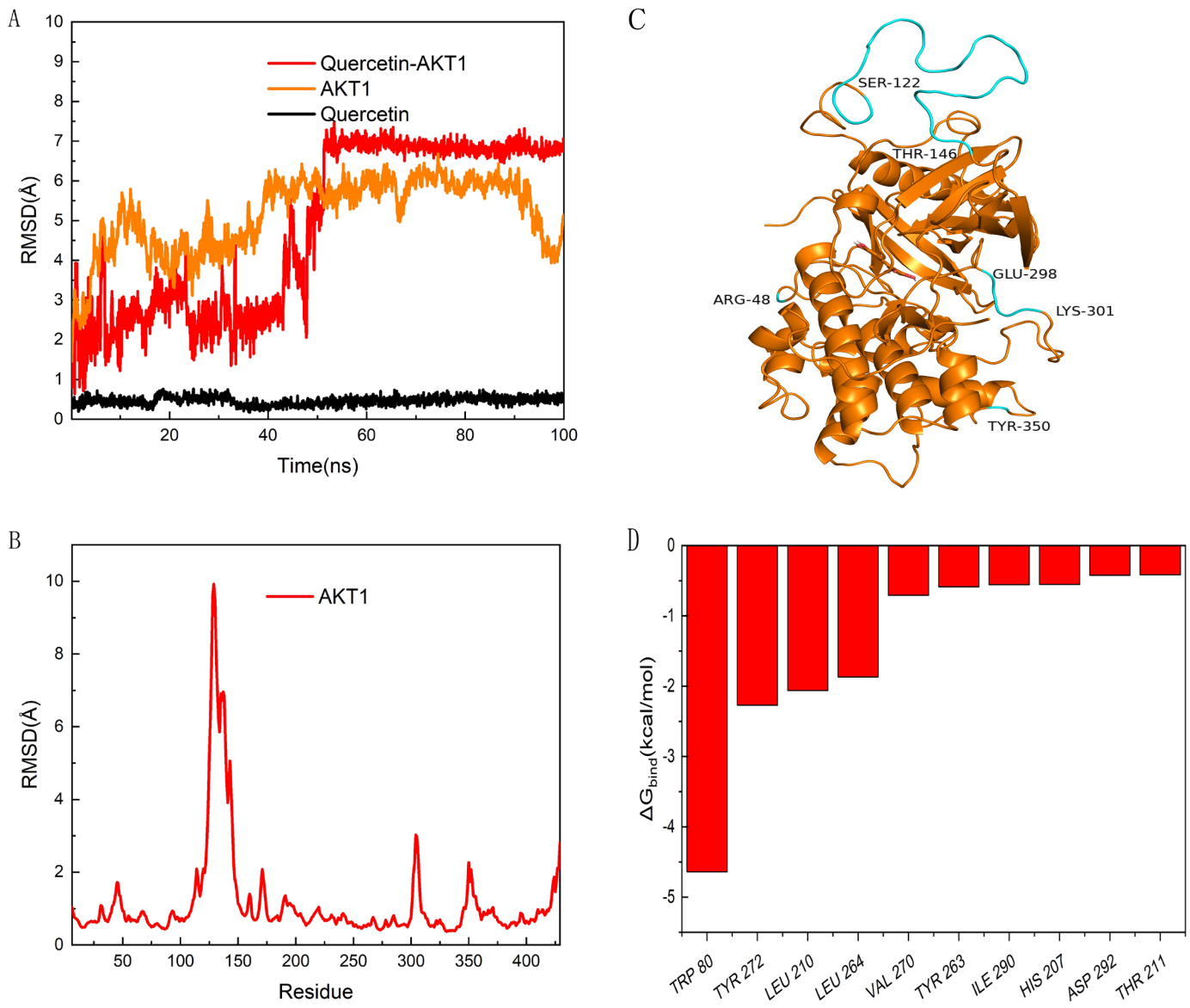

Figure 4: Results of MD simulation, A. RMSD of the quercetin-AKT1 complex. B. RMSF analysis of AKT1. C. Structure of the quercetin-AKT1 complex at the end of simulation. D. Binding free energy decomposition per residue.

align with established pharmacophores for α-glucosidase inhibition, providing a structure-activity rationale for the potent *in vitro* activity observed (Liu *et al.*, 2025). PPI network analysis pinpointed central targets such as AKT1, TNF, and IL6, which are critically involved in insulin signaling, inflammatory cascades, and metabolic homeostasis. For instance, AKT1 is a pivotal kinase in the PI3K/Akt pathway, promoting GLUT4 translocation and glucose uptake upon activation (Salem *et al.*, 2025), while TNF and IL6 are core mediators of inflammation-induced insulin resistance in T2DM (Min *et al.*, 2025). This implies that loquat flower may not only directly curb carbohydrate digestion but also potentially ameliorate insulin resistance systemically by attenuating inflammatory signaling, consistent with the mild, multi-target regulatory profile desirable in functional foods.

GO and KEGG enrichment analyses further corroborated this holistic mechanism. Significant enrichment in biological processes like "response to hormone stimulus" and pathways such as "Lipid and atherosclerosis" underscores the potential intervention in core pathophysiological aspects of T2DM—metabolic dysregulation and chronic inflammation. The interconnection of these pathways highlights the role of insulin resistance and inflammation as "common soil" linking metabolic and cardiovascular diseases. Collectively, these findings suggest that the anti-T2DM benefits of loquat flower may extend beyond direct enzyme inhibition to a systemic action, likely mediated by the synergistic effects of its multiple components, which collectively could modulate insulin signaling and suppress metabolic inflammation, thereby addressing a fundamental aspect of T2DM pathology. Molecular docking verified robust

binding (affinity < -7 kcal/mol) between the core components and key targets, offering structural validation for the predicted interactions. ADMET predictions further support the therapeutic potential, indicating favorable gastrointestinal absorption and overall low toxicity for the main active constituents. However, the marginal predictions for carcinogenicity and mutagenicity associated with certain flavonoids (*e.g.*, quercetin) warrant careful long-term safety evaluation. Subsequent development should adhere to regulatory standards, establish safe dosing thresholds, and consider formulation strategies to mitigate potential risks.

The molecular docking predictions were further substantiated and refined by all-atom MD simulations. While docking suggested a favorable binding pose, the 100-ns MD simulation provided critical dynamic evidence of the exceptional stability of the quercetin-AKT1 complex. The remarkably low ligand RMSD (~0.5 Å) confirmed a tightly bound state, and the strong binding affinity was quantified by MM/GBSA calculations (ΔGbind = -43.06 kcal/mol). Crucially, the simulations provided an atomistic mechanistic explanation, suggesting the physical basis of this strong interaction. Energetic decomposition revealed that the binding was primarily driven by van der Waals forces, with key hydrophobic residues (TRP80, LEU210, TYR272) forming a complementary pocket. A critical π-π stacking interaction with TRP80 was identified as a central stabilizing factor. Thus, the MD simulations move beyond static docking, offering a superior understanding of the potential binding mechanism and representing a key methodological advancement in this study.

This study demonstrates the significant value of an integrative methodology in natural product research. By sequentially combining *in vitro* screening, network-based prediction, molecular docking, and dynamic simulation, we have established a robust workflow that bridges traditional ethnopharmacological knowledge and modern computational biology. This approach not only confirmed the direct enzyme inhibitory activity but also yielded novel mechanistic insights, moving beyond the conventional focus on α-glucosidase to propose AKT1 and inflammatory targets like TNF as potential central nodes in loquat flower's anti-T2DM action, thereby providing a more comprehensive systems-level understanding. The findings from this work offer tangible benefits for multiple stakeholders. For patients and at-risk individuals, it provides a scientific basis for the potential use of loquat flower as a dietary adjunct for glucose management. For agricultural and industrial sectors, the identified active batches and components pave the way for standardizing extracts to ensure consistent efficacy. The immediate translational step emerging from this study is the development of standardized loquat flower extracts based on the potent batch L12, guided by the quantified activity and phytochemical profile. Subsequent research should focus on validating the predicted mechanisms in human-relevant cell-based assays and pre-clinical models to further de-risk and guide future clinical evaluation.

Despite the insightful findings, this study has limitations. The network pharmacology predictions rely on public databases and computational models, requiring experimental validation. The *in vitro* enzyme inhibition assay, while indicative, cannot fully replicate the complex physiological environment *in vivo*. Lastly, the MD simulation, although informative, was conducted in a simplified system without considering the full cellular context. Based on these findings and limitations, we have outlined a clear trajectory for future research. First, the key flavonoid and triterpenoid components will be isolated and purified from the most active batch (L12) to directly validate their efficacy in improving glucose consumption in an insulin-resistant HepG2 cell model. Subsequently, the underlying mechanism will be experimentally investigated using techniques such as Western Blot to determine whether the extract can upregulate the phosphorylation of AKT1 at Ser473, thereby examining its potential modulatory effect on the PI3K/Akt pathway. Finally, the *in vivo* antidiabetic efficacy and overall safety profile will be comprehensively evaluated in T2DM animal models (*e.g.*, db/db mice), including systematic sub-chronic toxicity studies.

CONCLUSION

In conclusion, this integrated study demonstrates that loquat flower extract possesses significant α-glucosidase inhibitory activity, supporting its potential to modulate postprandial blood glucose. The combination of network pharmacology and molecular docking suggests a complex, multi-target mechanism, wherein core constituents like quercetin and ursolic acid are predicted to interact with key targets such as AKT1, TNF, and IL6. This network implicates potential modulation of pathways critical to insulin signaling and inflammatory response, offering a plausible systems-level explanation for its anti-diabetic effects beyond mere enzyme inhibition. Most importantly, MD simulations and MM/GBSA calculations provide atomistic-level evidence that the predicted binding between quercetin and AKT1 is highly stable and primarily facilitated by van der Waals interactions, with a central contribution from a π-π stacking interaction with TRP80.

Collectively, this work provides a modern scientific rationale for the traditional use of loquat flower and establishes a robust theoretical framework for its future development as a functional ingredient. The findings, however, remain largely predictive and computational. Therefore, subsequent research is imperative to empirically validate these insights, focusing on the isolation and quantification of the active compounds, *in vivo* confirmation of efficacy and safety, and experimental verification of the proposed target engagements and mechanistic pathways.

ABBREVIATIONS

IC_{50}: Half-maximal inhibitory concentration; **ΔSASA:** Change in solvent-accessible surface area (used in calculating non-polar solvation energy); **OMIM:** Online Mendelian Inheritance in Man (database for disease-associated targets); **AKT1:** Protein Kinase B (core target); **TP53:** Tumor Protein 53 (core target); **STAT3:** Signal Transducer and Activator of Transcription 3 (core target); **TNF:** Tumor Necrosis Factor (core target); **IL6:** Interleukin 6 (core target); **ESR1:** Estrogen Receptor 1 (core target); **MAPK1:** Mitogen-Activated Protein Kinase 1 (core target); **IL1B:** Interleukin 1 Beta (core target); **CASP3:** Caspase 3 (core target); **BCL2:** B-cell Lymphoma 2 (core target).

CONFLICT OF INTEREST

The authors declare that there is no conflict of interest.

FUNDING

This research was funded by the General scientific research project of Zhejiang Provincial Department of Education (No. Y202147756).

AUTHOR CONTRIBUTIONS

Hanhua Wang: conceptualization, methodology, software, writing - original draft. Sisi Zeng: data curation, supervision, visualization. Yanyue Wang: resources, investigation, writing - reviewing and editing.

DATA AVAILABILITY STATEMENT

The data that support the findings of this study are available from the corresponding author upon reasonable request.

SUMMARY

This study integrates multiple methodologies to demonstrate that Eriobotrya japonica flower exhibits anti-T2DM activity through α-glucosidase inhibition and multi-target mechanisms. Molecular dynamics simulations confirmed the stable binding of quercetin to AKT1, providing a pharmacodynamic basis for its potential development as an anti-diabetic agent.

REFERENCES

Araki E, Tanaka A, Inagaki N, Ito H, Ueki K, Murohara T, Node K. (2021). Diagnosis, prevention, and treatment of cardiovascular diseases in people with type 2 diabetes and prediabetes. *Diabetol Int, 12*(1), 1–51. https://doi.org/10.1007/s13340-020-00471-5

Chen B, Long P, Sun Y, Meng Q, Liu X, Cui H, Zhang, L. (2017). The chemical profiling of loquat leaf extract by HPLC-DAD-ESI-MS and its effects on hyperlipidemia and hyperglycemia in rats induced by a high-fat and fructose diet. *Food Funct*, *8*(2), 687–694. https://doi.org/10.1039/c6fo01578f

Chen Q, Tao W, Zheng M, Ma Z, Wang L, Lu S. (2023). Optimization of ethanol extraction and purification process of loquat flowers based on *in vitro* tyrosinase inhibitory activity and preliminary identification of active components. *Acta Agric Zhejiang*, *35*(5), 1144–1153. (in Chinese) https://doi.org/10.3969/j.issn.1004-1524.2023.05.18

Consortium UniProt. (2023). UniProt: the universal protein knowledgebase in 2023. *Nucleic Acids Res*, *51*(D1), D523–D531. https://doi.org/10.1093/nar/gkac1052

Davis AP, Wiegers TC, Johnson RJ, Sciaky D, Wiegers J, Mattingly CJ. (2023). Comparative toxicogenomics database: update 2023. *Nucleic Acids Res*, *51*(D1), D1257–D1262. https://doi.org/10.1093/nar/gkac833

Duan M, Feng J, Feng J, Wang X, Xiao X, He S, Rao MJ. (2025). Optimizing processing methods for maximum bioactive retention: comparative metabolomic analysis of dried loquat flowers and their powdered extracts. *Front Nutr*, *12*, 1637247. https://doi.org/10.3389/fnut.2025.1637247

Flachsenberg F, Ehrt C, Gutermuth T, Rarey M. (2024). Redocking the PDB. *J Chem Inf Model*, *64*(1), 219–237. https://doi.org/10.1021/acs.jcim.3c01573

Huang J, Wen J, Wu F, Zhou P, Zhang J, Wang L, Li, H. (2025). Comparative transcriptomic analysis of loquat floral fragrance and hormone synthesis regulation across developmental stages. *Front Plant Sci*, *16*, 1574771. https://doi.org/10.3389/fpls.2025.1574771

Kim S, Chen J, Cheng T, Gindulyte A, He J, He S, Bolton EE. (2025). PubChem 2025 update. *Nucleic Acids Res*, *53*(D1), D1516–D1525. https://doi.org/10.1093/nar/gkae1059

Li X, Miao F, Xin R, Tai Z, Pan H, Huang H, Zhu Q. (2023). Combining network pharmacology and molecular simulations to examine FHB granules on vitiligo. *Front Immunol*, *14*, 1194823. https://doi.org/10.3389/fimmu.2023.1194823

Li Y, Wang Z, Mei C, Sun W, Yuan X, Wang J. (2025). Phytochemical profiling and α-amylase/α-glucosidase inhibitory effects of 29 faba bean varieties. *Biology*, *14*(8), 982. https://doi.org/10.3390/biology14080982

Liu S, Cai Y, Chen W, Yuan X, He Z, Lin F. (2025). Mechanistic study of quercetin in thyroid cancer with diabetes. *Front Endocrinol*, *16*, 1537799. https://doi.org/10.3389/fendo.2025.1537799

Luo J, Shu Y, Zhang W. (2023). Pharmacogenomics and pharmacomicrobiomics in type 2 diabetes mellitus. *Front Endocrinol*, *14*, 1287807. https://doi.org/10.3389/fendo.2023.1287807

Ma X, Huo Z, Shi M, Wang H, Yang T, Xiao J. (2025). Uncovering mechanisms of *Pholiota adiposa* in Alzheimer's disease. *Sci Rep*, *15*(1), 27981. https://doi.org/10.1038/s41598-025-94861-x

Min R, Aryani SS, Okti NP, Rini MP. (2025). Effect of *Hedyotis corymbosa* extract on pro-inflammatory cytokines. *BIO Web Conf*, *171*, 03018. https://doi.org/10.1051/bioconf/202517103018

National Health Commission of the People's Republic of China (2019) Announcement on new food ingredients (No. 2 [2019]). Retrieved from https://zwfw.nhc.gov.cn/kzx/tzgg/xspylsp_225/201905/t20190529_1261.html

Odhiambo, O. D., Omosa, K. L., Njagi, C. E., Kithure, G. J., & Wekesa, N. E. (2025). *In silico* ADME/Tox analysis of phytochemicals from genus Dracaena. *Sci Afr*, *29*, e02796. https://doi.org/10.1016/j.sciaf.2025.e02796

Ru J, Li P, Wang J, Wei Z, Li B, Chao H. (2024). TCMSP: a database of systems pharmacology for drug discovery from herbal medicines. *J Cheminform*, *6*, 13. https://doi.org/10.1186/1758-2946-6-13

Sabarathinam S, Satheesh S. (2025). Unveiling molecular mechanisms of maslinic acid in diabetes. *Aspects Mol Med*, *5*: 100060. https://doi.org/10.1016/j.amolm.2024.100060

Salem E, Ta A, Fueger PT, Wang PH. (2025). Dual roles of renal tubular mitochondrial AKT1 in glucose metabolism. *Diabetes*, *74*(S1), 1. https://doi.org/10.2337/db25-380-P

Singh N, Jogana AZ, Khanna S. (2025). Theoretical and experimental approaches to thiosemicarbazone. *Phosphorus*, *200*(9), 694–705. https://doi.org/10.1080/10426507.2025.2541791

Sun H, Saeedi P, Karuranga S, Pinkepank M, Ogurtsova K, Duncan BB, Magliano JD. (2022). IDF Diabetes Atlas: Global diabetes prevalence estimates for 2021. *Diabetes Res Clin Pract*, *183*, 109119. https://doi.org/10.1016/j.diabres.2021.109119

Szklarczyk D, Nastou KC, Koutrouli M, Kirsch R, Mehryary F, Hachilif R, von Mering C. (2025). The STRING database in 2025. *Nucleic Acids Res*, *53*(D1), D730–D737. https://doi.org/10.1093/nar/gkae1113

Wahjudi NP, Lu Q, Patterson EM, Zhang X, Go VL, Chen J, Lee WNP. (2017). Anti-hyperglycemic effect of loquat leaf extract. *Metabolomics*, *13*(8), 91. https://doi.org/10.1007/s11306-017-1228-5

Wang H, Ruan H, Chen Y. (2019). Research progress on chemical constituents and pharmacological effects of loquat flower. *Chin Tradit Patent Med*, *41*(12), 2977–2981. (in Chinese) https://doi.org/10.3969/j.issn.1001-1528.2019.12.030

Wang H, Yang X, Chen, Y. (2019). Antitussive, expectorant and anti-inflammatory activities of loquat flower extracts. *Chin J Gerontol*, *39*(6), 1431–1434. (in Chinese) https://doi.org/10.3969/j.issn.1005-9202.2019.06.048

Wang H, Yang X, Cui M, Li K, Chen H. (2018). Anti-inflammatory and antibacterial effects of *Fritillaria thunbergii* and loquat flowers. *Chin Tradit Patent Med*, *40*(1), 46–50. (in Chinese) https://doi.org/10.3969/j.issn.1001-1528.2018.01.008

Xie, C., & Ren, J. (2023). Network pharmacology in research on efficacy of traditional Chinese medicine. *Chin J Exp Tradit Med Form*, *30*(1),198–207. https://doi.org/10.13422/j.cnki.syfjx.20231516

Xiong X, Wang J, Nong Y, Cao W, Wang J, Xue C. (2025). Development and hypoglycemic efficacy of corn silk composite tea bags. *FST*, *50*(4), 123–131. https://doi.org/10.13684/j.cnki.spkj.2025.04.037

Yamada K, Hosokawa M, Fujimoto S, Fujiwara H, Fujita Y, Harada N, Inagaki N. (2008). Effect of corosolic acid on gluconeogenesis in rat liver. *Diabetes Res Clin Pract*, *80*(1), 48–55. https://doi.org/10.1016/j.diabres.2008.01.006

Yan B, Liao P, Han Z, Zhao J, Gao H, Liu Y, Lei P. (2025). Association of aging related genes and immune microenvironment with depression. *J Affect Disord*, *369*, 706–717. https://doi.org/10.1016/j.jad.2024.10.053

Zeka K, Ruparelia KC, Arroo RRJ, Budriesi R, Micucci M. (2017). Flavonoids and their metabolites: prevention in cardiovascular diseases and diabetes. *Diseases*, *5*(3), 19. https://doi.org/10.3390/diseases5030019

Zhang P, Zhang D, Zhou W, Wang B, Zhang T, Li S. (2023). Network pharmacology: towards AI-based precision traditional Chinese medicine. *Brief Bioinform*, *25*(1), bbad518. https://doi.org/10.1093/bib/bbad518

Zhang, J., Zhao, M., Wu, F., Shi, Z., & Xie, R. (2025). Inhibition mechanism of wedelolactone against α-glucosidase. *J Enzyme Inhib Med Chem*, *40*(1), 2551970. https://doi.org/10.1080/14756366.2025.2551970

Zhao L, Zhang H, Li N, Chen J, Xu H, Wang Y, Liang Q. (2023). Network pharmacology reveals pharmacology mechanism of Chinese medicine formula. *J Ethnopharmacol*, *309*, 116306. https://doi.org/10.1016/j.jep.2023.116306

Zhou S, Zhang Z, Li S, Liu M, Zhang Z, Wang N, Sun J. (2025). Characterization of α-glucosidase inhibitory peptides from peanut meal. *Food Res Int*, *218*, 116864. https://doi.org/10.1016/j.foodres.2025.116864

Zhou Y, Zhou B, Pache L, Chang M, Khodabakhshi AH, Tanaseichuk O, Chanda SK. (2019). Metascape resource for the analysis of systems-level datasets. *Nat Commun*, *10*(1), 1523. https://doi.org/10.1038/s41467-019-09234-6

Zhu F, Wu M, Kong X, Fang L, Ma Q, Tao, Y. (2022). Network mining of *Anoectochilus roxburghii* in type 2 diabetic mellitus. *Chin Tradit Herbal Drugs*, *53*(12), 3720–3729. (in Chinese) https://doi.org/10.7501/j.issn.0253-2670.2022.12.018

Cite this article: Wang H, Zeng S, Wang Y. Combining Experimental and Computational Approaches to Elucidate the Anti-T2DM Potential of *Eriobotrya japonica* Flower: *In vitro* Enzyme Inhibition, Network Pharmacology, Molecular Docking, and Molecular Dynamics Simulation. Pharmacog Res. 2026;18(3):829-42.